Title page

Gut microbiota-derived gamma-aminobutyric acid from metformin treatment reduces hepatic ischemia/reperfusion injury through inhibiting ferroptosis

Running title: Metformin against hepatic ferroptosis via microbial GABA

Fangyan Wang[+,1]; **Xiujie Liu**[+,1,4]; **Furong Huang**[+,1]; Yan Zhou[2]; Xinyu Wang[1]; Zhengyang Song[1]; Sisi Wang[1]; Xiaoting Wang[1]; Dibang Shi[3]; Gaoyi Ruan[3]; Xiawei Ji[3]; Eryao Zhang[3]; Zenglin Tan[1]; Yuqing Ye[4]; Chuang Wang[5]; **Jesse Zhu***[,4]; **Wantie Wang***[,1]

[1]*Institute of ischemia/reperfusion Injury; School of basic medical science, Wenzhou Medical University, Wenzhou, China;* [2]*Wenzhou Key Laboratory of Sanitary Microbiology; Wenzhou Medical University, Wenzhou, China;* [3]*Department of Gastroenterology, The Second Affiliated Hospital and Yuying Children's Hospital of Wenzhou Medical University, Wenzhou, China;* [4]*Nottingham Ningbo China Beacons of Excellence Research and Innovation Institute, The University of Nottingham Ningbo, Ningbo; Suzhou Inhal Pharma Co., Ltd., Suzhou, China;* [5]*Medical school of Ningbo University, Ningbo University, Ningbo, China.*

[+]These authors contributed equally to this work and share first authorship.

*Corresponding Author: Prof. Wantie Wang Email: wwt@wmu.edu.cn;

Prof. Jesse Zhu Email: jzhu@uwo.ca

Metformin mitigates hepatic ischemia/reperfusion-induced ferroptosis via gamma-aminobutyric acid derived from reshaped gut microbiota

Abstract: Hepatic ischemia/reperfusion injury (HIRI) is a common and inevitable factor leading to poor prognosis in various liver diseases, making the outcomes of current treatments in clinic unsatisfactory. Metformin has been demonstrated to be beneficial to alleviate HIRI in recent studies, however, the underpinning mechanism remains unclear. In this study, we found metformin mitigates HIRI-induced ferroptosis through reshaped gut microbiota in mice, which was confirmed by the results of fecal microbiota transplantation (FMT) treatment but showed the elimination of the beneficial effects when gut bacteria were depleted using antibiotics. Detailedly, through 16S rRNA and metagenomic sequencing, we identified that the metformin-reshaped microbiota was characterized by the increase of gamma-aminobutyric acid (GABA) producing bacteria. This increase was further confirmed by the elevation of GABA synthesis key enzymes, glutamic acid decarboxylase (GAD) and putrescine aminotransferase (PAT), in gut microbes of metformin-treated mice and healthy volunteers. Furthermore, the benefit of GABA against HIRI-induced ferroptosis was demonstrated in GABA-treated mice. Collectively, our data indicate that metformin can mitigate HIRI-induced ferroptosis by reshaped gut microbiota, with GABA identified as a key metabolite.

Keywords: ferroptosis / gamma-aminobutyric acid / gut microbiota / hepatic ischemia-reperfusion injury / metformin

Introduction

Hepatic ischemia/reperfusion injury (HIRI) remains a major cause of liver damage mainly following liver transplantation, complicated hepatectomy, haemorrhagic shock and severe liver trauma.[1-4] Traditional therapeutics have been developed and repurposed to treat HIRI, including ischemic preconditioning, machine perfusion technologies, gene interventions, and stem cell therapy.[5-8] Unfortunately, current treatments are not satisfactory due to the complicated pathogenesis of HIRI. Recently, a novel theory relating to the gut-liver axis has been well accepted, demonstrating that gut microbiota is vital for liver diseases, however, there is no strategy targeted this theory to alleviate HIRI in clinical practice.

The liver links with the intestine by portal circulation which allows the transfer of gut-derived products, not only nutrients, but also microbial metabolites and components.[9] As an important part of the gut-liver communication, the intestinal mucosal and vascular barriers limit the systemic dissemination of microbes and toxins while allowing nutrients to access the circulation and reaching the liver.[10] Additionally, it is generally believed that liver injury can provoke intestinal mucosal damage and inflammation, further resulting in gut dysbiosis, which reversely induces a secondary attack on the liver.[11] Microbial agents, such as synbiotics and probiotics, have demonstrated to attenuate different liver diseases in animal studies,[12, 13] indicating that modulating gut microbes potentially prevents HIRI in clinical practice.

Recently, the hypoglycaemic drug, metformin, has attracted intensive attention in its pleiotropic biological actions in various diseases, such as obesity, cancer, nuroinflammation, especially liver diseases.[14-17] As evidences shown, the gut with high concentration of metformin become an important action site to reshape microbiota.[18] According to *Sun et al.*,[19] metformin was proven to decrease the abundance of the *B. fragilis* species and to increase the levels of bile acid and glycoursodeoxycholic acid in the gut, which inhibited intestinal farnesoid X receptor against obesity-related metabolic dysfunction in mice. Moreover, it is also demonstrated that metformin could attenuate sepsis-related liver injury by increasing the proportion of *Bifidobacterium*,

Muribaculaceae, *Parabacteroides distasonis*, and *Alloprevitella* in rats.[20] As for the HIRI, metformin has also shown the protective effect,[21] but the detailed role of gut microbiota remains unclear.

Although metformin showed protective effects on HIRI, the role and distinctions of reshaping microbes have yet to be determined. In the present study, we sought to elucidate that gamma-aminobutyric acid (GABA)-producing bacteria played a critical role for the protective effects of metformin against HIRI by using 16S rRNA and metagenomic sequencing to find the different features of gut microbiota. The finding was reconfirmed by the results of mice that were treated with metformin-reshaped fecal microbiota or oral antibiotics administration. Furthermore, GABA was found to show a protective effect on HIRI by intraperitoneally injection into mice in advance, while an increase of microbial GABA was observed in both mice and human experiments after metformin treatment. Evidenced by the improvement of HIRI, we hypothesize that metformin-reshaped gut microbiota elicits greater therapeutic responses for liver diseases and serve as a promising targeted therapeutic.

Results

Metformin significantly mitigates HIRI and reshapes gut microbiota in mice

In order to evaluate the protective effect of metformin on HIRI, survival experiment was employed in mice. The survival rate of HIRI mice increased from 41.67% to 90.00% after metformin intervention (Fig. 1a), accompanied by hepatic morphological and histopathological improvement including the recovery of liver pathological structure, the decrease in red blood cell aggregation and consumption of liver glycogen (Fig. 1b), as well as the decrease in serum activity of ALT and AST (Fig. 1c). Qualification of MDA and GSH concentrations in the mice liver demonstrated that the presence of metformin significantly attenuated HIRI-induced oxidation (Fig. 1d).

In order to clarify the critical role of gut microbiota in the pleiotropic actions of metformin,[22-24] fecal samples were collected from the mice to perform 16S rRNA sequencing. It was found that the gut microbiota was substantially modulated in IR + metformin (Met) group, showing decreased abundance (alpha diversity) and reshaped distribution (Fig. 1e). Next, as the microbiota-gut-liver axis theory indicates,[25] HIRI-induced dysfunction of the gut barrier may aggravate liver damage by disrupting the gut microbiota. H&E staining of the colon and ileum, mainly involved in gut barrier dysfunction, showed that the density and integrity of intestinal mucosa were strikingly reduced by HIRI, which was restored by metformin treatment (Fig. 1f). The immunofluorescence analysis of colon tissues showed that the decreased tight junction protein ZO-1 and Occludin in HIRI-treated mice were reversed by metformin (Fig. 1g and 1h). Similarly, western blot analysis of Occludin in colon (Fig. 1g) and the mRNA levels of *Ocln*, *Tjp1*, *Cldn7*, *F11r* and *Igsf5* in ileum of HIRI mice were increased with metformin administration (Fig. 1i). The inflammatory cytokine *Il6*, *Il1b* and *Il18* were significantly upregulated in the ileum and colon received HIRI and were reduced by metformin treatment (Fig. 1j). In addition, the serum FD-4 level in IR group was cut down by metformin (Fig. 1k). These results suggested that metformin plays a critical role in restoring gut barrier function and alleviating HIRI.

Metformin-reshaped fecal microbiota attenuates HIRI

In order to further confirm the role of metformin in reshaping the gut microbiota, microbes were transplanted into mice before inducing ischemia reperfusion (IR). As expected, the survival analysis of mice in the IR + fecal microbiota transplantation (FMT) group showed a similarly protective efficacy as the IR + Met group, as indicated by the significantly improved survival rate of IR mice (Fig. 2a). This finding was validated by ALT and AST levels as well as H&E, PAS and DHE staining (Fig. 2b and 2e). FMT treatment could restore the GSH level but reduce the accumulation of MDA in hepatic tissues (Fig 2c and 2d). Furthermore, a decreased alpha diversity was observed in the FMT group, similar to IR + Met group (Fig. 2f). Meanwhile, the attenuation of gut damage was showed by H&E staining, and the improvement in tight junction

proteins ZO-1 and Occludin, and decreased HIRI-induced *Il1b*, *Il6*, and *Il18* (Fig. 2g-2i). Serum FD-4 level showed a sharply decrease in IR + FMT group (Fig. 2j). To further identify the function of gut microbes, experiments were designed, and combination treatment of antibiotics (1 mg/mL penicillin sulfate, 1 mg/mL neomycin sulfate, 1 mg/mL metronidazole and 0.16 mg/mL gentamicin) and metformin were employed for 1 week before IR treated. As results showed, the ALT, AST and MDA detection in control group treated with Abx showed no obvious change to control group, indicating that the Abx had no influence on the liver. The survival rate of IR + Met + antibiotics (Abx) group was greatly reduced, while the levels of ALT, AST, MAD and GSH were completely opposite to IR + Met group (Fig. 2k). The results confirmed that gut microbiota is critical for the effect of metformin against HIRI.

FMT alleviates HIRI-induced ferroptosis through reshaped fecal microbiota

Since the reperfusion-induced excessive oxidative stress takes place in iron-rich hepatocytes,[26] experiments were designed to observe ferroptosis in HIRI. The ferroptosis inhibitor, DFO, significantly ameliorated the liver injury, suggesting that ferroptosis contributes to HIRI (sFig. 1). Hence, to find out the relation, ferroptosis-related indicators were also monitored in both IR + Met and IR + FMT groups. The increased accumulation of Fe after HIRI was significantly cut down by metformin and FMT treatment (Fig. 3a). The quantitative Real-time PCR (qRT-PCR) analysis showed that the HIRI-induced upregulation of ferroptotic parameters, *Acsl4*, *Slc7a11*, *Slc39a14* and *Ptgs2*, were significantly decreased by metformin and its reshaped gut microbiota, respectively (Fig. 3b-3e). The results of western blotting further confirmed the anti-ferroptosis of metformin and FMT by the remarkable reduction of ACSL4, TFR1, VDAC1, VDAC2 and VDAC3 levels and the apparent increase of antiferroptotic FTH1 and Xct levels (Fig. 3f), The results were further consolidated by lipid ROS staining and transmission electron microscopy (TEM) analysis (Fig. 3g). Additionally, transcriptome data on genes associated with antiferroptosis showed an increase in both IR + Met and IR + FMT groups, whereas proferroptic genes showed a decrease, when compared with IR group (Fig. 3h). Collectively, the results suggested that FMT performed protection against HIRI by inhibiting ferroptosis.

Metformin induces GABA-producing gut microbiota

To elucidate the molecular mechanisms through which pathway participates metformin-treated IR injury, we analysed gene expression profiles of each group mice. Transcriptome sequencing analysis revealed that 9697 genes were in common among four groups (sfig. 6). Therefore, we used these common genes for KEGG analysis, showing that similar mRNA changes are mainly concentrated in the three top pathways: lipid metabolism, carbohydrate metabolism, and amino acid metabolism (Fig 4a). Given the close relevance between lipid metabolism and ferroptosis (sFig. 2), and the fact of carbohydrate metabolism is a primary way to metabolize amino acids, 22 species of amino acid were detected in liver tissues using HPLC-MS/MS for further identification of key metabolites involved in the role of metformin against HIRI-induced ferroptosis. It was found that only GABA level is significantly increased by metformin treatment and FMT treatment (sFig. 3), further verifying by the data of ELISA detection (Fig. 4b). Moreover, it was observed that the genus of *Bacteroides* had a significant increase based on the 16s rRNA gene sequencing of metformin-treated mice microbes. qRT-PCR analysis of eukaryotic GABA synthesis key enzymes including *Aldh5a1*, *Abat*, *Gad1* and *Gad2* in liver tissues, were not upregulated by metformin (Fig. 4d), which was also confirmed by western blotting detection of GAD1 and GAD2 in liver (Fig. 4f). Interestingly, the fecal GABA concentration was shown a significant increase in metformin-treated mice, which was copied by the IR + FMT group, but eliminated by antibiotics treatment (Fig. 4e). In order to further identify the increased GABA originates from gut microbiota, two key enzymes of prokaryotes GABA synthesis, GAD and PAT, were detected on DNA level, finding that both of them are significantly increased in the feces from IR+Met and IR+FMT groups (Fig. 4g and h). In order to clarify the specific effects of metformin on microbiota, given the big safety margin, healthy volunteers were recruited for a 1 week of daily oral 500mg dose of metformin trial. Fecal samples were collected before and after oral administration of metformin for metagenomic analysis. Detailedly, the species of Bacteroides containing Bacteroides thetaiotaomicron, Bacteroides unifomis, and Bacteroides salyersiae, were enriched in human gut after metformin

administration (Fig. 4i). Excitingly, the increase of GABA production, and the expression of GAD and PAT were shown in the results of fecal experiments *in vitro* and *in vivo*, accompanied by the decreased glutamic acid (Glu), a key substrate for gut microbiota to synthesize GABA (Fig. 4j and k). Besides, putrescine, another substrate of GABA synthesis, was not found in primary culture medium but appeared after 24h fermentation and then was consumption later in the anaerobic culture of human feces experiment. (Fig. 4l). Taken collectively, GABA-producing gut microbiota was upregulated by metformin.

GABA is the critical metabolite of metformin-reshaped gut microbiota against HIRI-induced ferroptosis

The animal experiment was designed to further observe the effects of GABA on HIRI-induced ferroptosis (Fig. 5a). As expected, the data showed that GABA treatment reduced histological damage and liver glycogen consumption (Fig. 5b). Serum liver function detection showed that ALT and AST activities were dramatically depressed after GABA treatment (Fig. 5c). The decreased MDA and Fe as well as increased GSH were observed in further determination, confirming the protection of GABA on liver (Fig. 5d). The results of western blotting showed the anti-ferroptosis effect of GABA treatment by the significant reduction in ACSL4, TFR1, VDAC1,2,3 and increase of anti-ferroptotic FTH1 levels, which had the same attenuating effect as metformin and FMT treatment (Fig. 5e). In addition, the clustergram showed GABA upregulated the genes of antiferroptosis and depressed the proferroptic ones, which was similar to the effect after metformin treatment (Fig. 5f). In summary, GABA treatment reduced HIRI-induced ferroptosis.

Discussion

Metformin has been well researched for treating various liver diseases due to its multifarious effects. Notably, it has been well documented that oral administration of metformin lead to therapeutic effects on HIRI,[27] leaving a thought-provoking question in its underlying mechanism. In the current study, the changes in the gut microbiota altered by metformin are

demonstrated to be necessary and sufficient for conferring liver injury protection. Moreover, it has been confirmed that metformin attenuated HIRI by the increased GABA from reshaped gut microbiota, through anti-ferroptosis.

Increasing evidence shows that the gut microbiota is critical for the pleiotropic actions of metformin.[25, 28, 29] Interestingly, metformin was previously found to have a much higher concentration in the gut lumen than other organs,[18] as also confirmed by the current study. In fact, that concentration favoured the action of metformin on reshaping gut microbes. Despite the distinct heterogeneity of metformin-reshaped gut microbiota in recent research, *Bacteroides* with a high abundance of gut microbes was reported to be reduced after metformin treatment in studies of hyperlipidemia and diabetes,[19, 30] which other studies vary from for the different action of this bacteria.[31, 32] In our study, we used a disease model of HIRI, which may have unique characteristics compared to other disease models. It is possible that the specific disease model influenced the response of the gut microbiota. Additionally, the starting microbiota of the recipients and the characteristics of the donor microbiota used for FMT could also play a role in the disparity. Our findings showed an increase abundance of the genus of *Bacteroides* after metformin treatment supported by the data of mice and healthy volunteers. Detailedly, the increased *Bacteroides* especially *Bacteroides thetaiotaomicron*, *Bacteroides unifomis,* and *Bacteroides salyersiae* were observed in the human gut after metformin administration. The enriched *Bacteroides theaiotaomicron*, a glutamate-fermenting commensal, was reported to be decreased in obese individuals and was inversely correlated with serum glutamate concentration.[33] Therefore, *Bacteroides theaiotaomicron* might be the potential bacterium regulating of GABA production. Little research has been done on *Bacteroides unifomis* and *Bacteroides salyersiae*, needing a further exploration of their characteristics in the future. Notably, *Phascolarctobacterium*, coexistly with *Bacteroides thetaiotaomicron,*[34] was reported as an emerging probiotic which showed a significant increase in our study. Taken collectively, those reshaped bacteria after metformin treatment may be responsible for attenuating HIRI.

Increased GABA was shown from the metformin reshaped gut microbiota for the first time, verified by our results of feces from mice and humans. As the critical metabolite of bacteria against acid stress, GABA was extensively produced by gut microbes, especially the species with strong capacity of acid resistance. Interestingly, our analysis of the sequences in PUBMED Gene bank found that those three species of *Bacteroides, Bacteroides thetaiotaomicron, Bacteroides unifomis, and Bacteroides salyersiae,* which belong to metformin reshaped microbiota, contain the key enzyme genes of GABA synthesis GAD and PAT (sFig 4), further confirmed by the qRT-PCR result of human fecal DNA *in vivo* and *in vitro* experiment. Specifically, the species with the strong ability of producing GABA such as *Bacteroides theaiotaomicron, Bacteroides unifomis and Bacteroides salyersiae* were increased in metformin-treated volunteers. Some studies were published to elucidate the mechanism of metformin regulating bile acids and folate metabolite by reshaped gut microbiota, however, there is no report about how metformin to affect GABA synthesis of gut microbes. The data from anaerobic cultured human feces showed that metformin promoted the increase of GAD and PAT, and GABA level along with the substrate consumption of glutamate and putrescine in a time-dependent manner.

GABA production was reported to be critical against acid stress for microbiota to survive and preserve metabolic activity, especially in the human gut with a lower pH than other animals.[35] Humans benefit from bacteria-derived GABA. Peripheral GABA was first demonstrated in intestinal flora in 1981 and further confirmed by recent studies.[36] In addition to the important role in the central neural system and immune system, GABA showed a protective effect in different acute liver injury models.[37, 38] Published papers have shown that GABA performs beneficial effect through binding to the GABA receptors or promoting histone acetylation.[39, 40] Our data from GABA-treated mice showed protective effects against HIRI-induced ferroptosis. However, further studies are required to examine the exact molecular mechanisms of GABA regulating ferroptosis.

In conclusion, we have demonstrated metformin-reshaped gut microbiota performs therapeutic responses for HIRI. Gut microbiota has been obviously modified while receiving oral metformin treatment, suggesting that metformin-reshaped gut microbiota has enhanced intestinal mucosal function so that reduce harmful substances to the liver, which most efficiently evade damage. Specifically, GABA producing bacteria were significantly regulated after metformin administration. Demonstrated for the first time, we showed that the increased GABA is a key metabolite of gut microbiota for metformin to mitigate HIRI. These results offer a unique therapeutic strategy, with optimized gut microbiota, that can serve as a target for metformin treating liver diseases.

Material and methods

Animals

Six-to-eight-week-old specific pathogen-free male C57BL/6 mice were purchased from Beijing Weitonglihua Experimental Animal Technology Co. Ltd. (Beijing, China). All mice were housed under controlled temperature and humidity conditions with a 12-h light–dark cycle and free access to food and water. The mice were fasted overnight before the experiments. All animal experiments were approved by the Institutional Animal Care and Use Committee of the Experimental Animal Centre of Wenzhou Medical University (wydw2021-0348).

Healthy volunteers

All research was conducted in accordance with both the Declarations of Helsinki and Istanbul, all research was approved by the Ethics Committee of the Second Affiliated Hospital of Wenzhou Medical University (2022-K-08-01), and written consent was given in writing by all subjects.

Hepatic ischemia/reperfusion (IR) mouse model

A mouse model for HIRI was established as previously described.[3] Briefly, mice were anaesthetised with pentobarbital sodium. A noninvasive microvascular artery clip was placed on the left branches of the hepatic artery and portal vein for 30 min, and the clip was removed for reperfusion for 6 h. During the study period, body temperature was maintained at 37 °C using a heating lamp.

Experimental design

Mice were randomly divided into the several groups. In general, the arterial and portal vessels to the cephalad lobes were clamped for 30min and reperfusion for 6 h. No vascular occlusion in sham-controlled mice. In the treatment groups, animals were treated with metformin (1 mg/mL), metformin modified fecal microbiota transplantation or metformin (1 mg/mL) mixed with antibiotics (1 mg/mL penicillin, 1 mg/mL neomycin sulfate, 1 mg/mL metronidazole and 0.16 mg/mL gentamicin), in the drinking water for 1 week. Specifically, FMT-treated mice were fed with washed metformin-treated mice feces, which had been detected by HPLC showing that there was no metformin left in the feces. Other two groups of mice were infused at 1 h prior to the onset of liver ischemia with a single dose of deferoxamine (DFO) (20 mg/kg i.p.) or GABA (100 mg/kg i.p.), dissolved in PBS. Mice were sacrificed after reperfusion; liver and serum samples were collected for analysis.

Measurement of serum alanine transaminase (AST), aspertate aminotransferase (ALT) level, liver Fe content and GABA level

Serum AST and ALT levels were measured using assay kits (Nanjing Jiancheng Bioengineering Institute, C010-2-1, C009-2-1). Liver samples were homogenised in saline, and Fe concentrations were measured by tissue Fe assay kit (Nanjing Jiancheng Bioengineering Institute, A039-2-1). GABA level was detected by an ELISA kit (Wuhan MSKBIO, KT21124).

Measurement of lipid peroxidation, glutathione (GSH) and superoxide anion levels of liver tissues

Malondialdehyde (MDA) Detection Kit (Nanjing Jiancheng Bioengineering Institute, A003-1-2) was determined to select the MDA level as a marker of lipid peroxidation. The assay was performed according to the manufacturer's instructions. Lipid reactive oxygen species (ROS) was measured by BODIPY 581/591 C11 (MKbio, 217075-36-0). Sections were stained with BODIPY 581/591 C11 and nucleated with 4',6-diamidino-2-phenylindole (DAPI) (Beyotime Institute of Biotechnology, A0131). Images were acquired under a fluorescence microscope (Nikon, Tokyo, Japan). The liver was homogenised, and the supernatant was collected for GSH analysis using a GSH assay kit (Nanjing Jiancheng Bioengineering Institute, A006). Frozen sections of the liver (8 μm) were placed on glass slides and incubated with 10 mmol/L dihydroethidium (DHE) (Beyotime Institute of Biotechnology, S0063) in a dark container at 37 °C for 30 min. Sections were rinsed three times in phosphate-buffered saline (PBS) then observed using an upright microscope (Nikon, Tokyo, Japan).

Hematoxylin-eosin (H&E) and periodic acid-schiff (PAS) staining

For histopathological examination, liver and intestinal tissues were fixed in 4% paraformaldehyde overnight. Selected tissue blocks were processed using a routine overnight cycle in a tissue processor. Tissue blocks were then embedded in wax and serially sliced into 5-μm sections. H&E and PAS staining performed as instructions provided by the reagent manufacturer (Solarbio, G1120, G1281). Visualization and images were obtained under an optical microscope (Nikon, Tokyo, Japan).

Histoimmunofluorescence staining

During immunofluorescence, sections were dyeing with primary antibody (1:100) Occludin (Proteintech, 27260-1-AP) and zonula occludens 1 (ZO-1) (Proteintech, 66378-1-IG) and incubated at 4°C overnight. Secondary antibody coupled with Alexa Fluor 488 (Bioss, bs-

40296G-AF488) was incubated at 37°C for 1 h. After additional PBS washing, the sections were sealed with an antifluorescence quencher containing 4',6-diamidino-2-phenylindole (DAPI). Immunofluorescence images were obtained using a laser scanning confocal microscope (Nikon, Tokyo, Japan) and quantified by ImageJ (NIH, USA).

Transmission electron microscopy (TEM) analysis

After reperfusion, the mice were euthanized, and the livers were excised and washed with precooled PBS (pH 7.4). Part of the liver was then removed and incubated overnight in 0.1 M PBS (pH 7.4) containing 2.5% glutaraldehyde. The target tissues were cut into 50-μm-thick sections using a vibratome. Selected areas of the livers were postfixed in 1% osmium tetroxide for 1 h, dehydrated in a graded ethanol series and embedded in epoxy resin. The polymerisation was performed at 80 °C for 24 h. Ultrathin sections (100 nm) were cut, stained with uranyl acetate and lead citrate and viewed under a JEM2000EX TEM (JEOL, Tokyo, Japan). Five fields were randomly selected for each sample to examine mitochondria with ferroptosis features.

Quantitative Real-time PCR (qRT-PCR) analysis

Total RNA was extracted from liver and intestinal tissues using TRIzol (Yamei, YY101). Isolated RNA was reverse transcribed to cDNA using a kit (Vazyme, R323-01). The obtained cDNA was subjected to PCR using primers designed to detect Interleukin *(Il)6, Il1b, Il18*, recombinant solute carrier family 7, Member 11 (*Slc7a11*), solute carrier family 39, member 14 (*Slc39a14*), acyl-CoA synthetase long-chain family member 4 (*Acsl4*), cyclooxygenase-2*(Ptgs2*), *Tjp1, Ocln, Cldn7*, Junctional adhesion molecule 1 (*F11r*), Junctional adhesion molecule 4 (*Igsf5*), succinic semialdehyde dehydrogenase (*Aldh5a1*), GABA transaminase (*Abat*), *Gad1*, *Gad2* and *Actb* (primer sequences are listed in sFig. 5). Gene expression was determined using the SYBR Green kit (Vazyme, Q711-02). All the results were normalised against β-actin expression using the Thermal Cycler Dice Real Time System (ABI QuantStudio6, Singapore).

Western blotting

Total protein samples were extracted from tissues using RIPA lysis buffer (Yamei, PC101). Protein concentrations were determined using a BCA protein detection kit (Yamei, ZJ101). Proteins were separated using 10% SDS-PAGE and transferred to polyvinylidene fluoride membranes. Membranes were blocked in 5% skimmed milk then incubated with the primary antibodies ACSL4 (AbCam, ab155282), Transferrin Receptor 1 (TFR1) (Abclonl, A5865), ferritin heavy chain (FTH1) (AbCam, ab65080), Occludin (Proteintech, 27260-1-AP), GAPDH (Proteintech, 0494-1-AP) and β-tubulin (Proteintech, 10068-1-AP) at 4 °C overnight. After washing three times with tris buffered saline, the membranes were incubated with appropriate anti-rabbit or anti-mouse secondary antibodies at room temperature for 1 h. Imprinting was observed using chemiluminescence (Yamei, SQ201) and an Odyssey imaging system (Li-Cor-Biosciences, NE, USA).

High-performance liquid chromatography with tandem mass spectrometric detection (HPLC–MS/MS) detection of metformin and liver amino acids

Sample separation was performed using a ZORBAX Eclipse XDB-C18 column (4.6 × 150 mm, Agilent, USA) using an injection volume of 5 μL. Metformin detection conditions are as follows: column temperature of 30°C, one mobile phase is NaH_2PO_4 (Sigma, V900060) containing 5 mmol/L sodium dodecyl sulfonate (Sigma, V900859) with pH 3.5 while the other mobile phase is acetonitrile (Aladdin, A104440). The metformin content in each sample was measured by HPLC (Agilent 1260, USA). Amino acid detection conditions are as follows: column temperature of 40°C, mobile phase A of 10% methanol/water (containing 0.1% formic acid), mobile phase B of 50% methanol/water (containing 0.1% formic acid) and flow rate of 0.4 mL/min. Mass spectrometry was performed using a triple quadrupole mass spectrometer with an ESI source in negative ionisation mode. High-purity nitrogen was used as the nebulising and drying gas. Quantification was performed in multiple reaction monitoring mode.

16S rRNA sequencing

16S rRNA amplicon sequencing was performed at Chunlab Inc. (Seoul, Korea) with MiSeq system (Illumina). Briefly, for preparation of MiSeq library amplicons, target gene (16S rRNA V3–V4 region) was amplified using338F (5'-ACTCCTACGGGAGGCAGCAG-3') and 806R (5'-GGACTACHVGGGTWTCTAAT-3') primers, using an ABI GeneAmp 9700 PCR thermocycler (ABI, CA, USA). The PCR product was extracted from 2% agarose gel and purified using the AxyPrep DNA Gel Extraction Kit (Axygen Biosciences, Union City, CA, USA) according to the manufacturer's instructions and quantified using a Quantus Fluorometer (Promega, USA). Normalization was performed the counts of individual OTUs in a sample by dividing the total counts of all OTUs within that sample followed by a multiplication by resulting in relative abundance expressed.

Metagenomic sequencing

Total genomic DNA was extracted from human fecal samples as mentioned in 16S rRNA sequencing. DNA extract was fragmented to an average size of about 400 bp using Covaris M220 (Gene Company Limited, China) for paired-end library construction. Paired-end library was constructed using NEXTflexTM Rapid DNA-Seq (Bioo Scientific, Austin, TX, USA). Adapters containing the full complement of sequencing primer hybridization sites were ligated to the blunt-end of fragments. Paired-end sequencing was performed on Illumina NovaSeq/Hiseq Xten (Illumina Inc., San Diego, CA, USA) at Majorbio Bio-Pharm Technology Co., Ltd. (Shanghai, China) using NovaSeq Reagent Kits/HiSeq X Reagent Kits according to the manufacturer's instructions (www.illumina.com).

Statistical analysis

GraphPad Prism version 9.0 (GraphPad Software, San Diego, CA) was used for statistical treatment. Experimental data were shown as the mean ± SD. Two-tailed unpaired *Student's t-test* and *one-way ANOVA* with *Tukey's* correction were used for all comparisons of mice-related

experiments. A P value < 0.05 was considered significant. The sample distribution was determined using a Kolmogorov–Smirnov normality test.

Acknowledgements

We appreciate the support of Suzhou inhal pharma Co., Ltd and Zhejiang Xiaolun Intelligent Manufacturing Co., Ltd. We also thank Shanghai Majorbio Bio-pharm Technology Co., Ltd for assisting with the 16S rRNA and metagenomics analysis, Suzhou Bionovogenes for helping with the HPLC-MS/MS analysis.

Disclosure and competing interests statement

All the authors had no potential conflict of interest to declare.

Data availability

The original contributions presented in the study are publicly available. Sequencing data have been uploaded to NCBI including 16s sequencing (PRJNA1045386), transcriptome sequencing (PRJNA1048138) and metagenomic sequencing (PRJNA1049568). Other data can be found here: https://pan.quark.cn/s/aca2e6ffcbdc

References

1. Ye L, He S, Mao X, Zhang Y, Cai Y, Li S. Effect of Hepatic Macrophage Polarization and Apoptosis on Liver Ischemia and Reperfusion Injury During Liver Transplantation. *Front Immunol*. 2020;11:1193. doi:10.3389/fimmu.2020.01193

2. Jiao Z, Liu X, Ma Y, et al. Adipose-Derived Stem Cells Protect Ischemia-Reperfusion and Partial Hepatectomy by Attenuating Endoplasmic Reticulum Stress. *Front Cell Dev Biol*. 2020;8:177. doi:10.3389/fcell.2020.00177

3. Liu Y, Lu T, Zhang C, et al. Activation of YAP attenuates hepatic damage and fibrosis in liver ischemia-reperfusion injury. *J Hepatol*. Oct 2019;71(4):719-730. doi:10.1016/j.jhep.2019.05.029

4. Liu T, Zhang Q, Mo W, et al. The protective effects of shikonin on hepatic ischemia/reperfusion injury are mediated by the activation of the PI3K/Akt pathway. *Sci Rep*. Mar 21 2017;7:44785. doi:10.1038/srep44785

5. Liu X, Chen H, Yan Z, et al. Remote liver ischemic preconditioning attenuates myocardial ischemia/reperfusion injury in streptozotocin-induced diabetic rats. *Sci Rep*. Jan 21 2021;11(1):1903. doi:10.1038/s41598-021-81422-1

6. Czigany Z, Lurje I, Schmelzle M, et al. Ischemia-Reperfusion Injury in Marginal Liver Grafts and the Role of Hypothermic Machine Perfusion: Molecular Mechanisms and Clinical Implications. *J Clin Med*. Mar 20 2020;9(3):846. doi:10.3390/jcm9030846

7. Ke B, Lipshutz GS, Kupiec-Weglinski JW. Gene therapy in liver ischemia and reperfusion injury. *Curr Pharm Des*. 2006;12(23):2969-2975. doi:10.2174/138161206777947669

8. Rowart P, Erpicum P, Detry O, et al. Mesenchymal Stromal Cell Therapy in Ischemia/Reperfusion Injury. *J Immunol Res*. 2015;2015:602597. doi:10.1155/2015/602597

9. Albillos A, de Gottardi A, Rescigno M. The gut-liver axis in liver disease: Pathophysiological basis for therapy. *J Hepatol*. Mar 2020;72(3):558-577. doi:10.1016/j.jhep.2019.10.003

10. Tripathi A, Debelius J, Brenner DA, et al. The gut-liver axis and the intersection with the microbiome. *Nat Rev Gastroenterol Hepatol*. Jul 2018;15(7):397-411. doi:10.1038/s41575-018-0011-z

11. Carbajo-Pescador S, Porras D, Garcia-Mediavilla MV, et al. Beneficial effects of exercise on gut microbiota functionality and barrier integrity, and gut-liver crosstalk in an in vivo model of early obesity and non-alcoholic fatty liver disease. *Dis Model Mech*. Apr 30 2019;12(5):dmm039206. doi:10.1242/dmm.039206

12. Roychowdhury S, Glueck B, Han Y, Mohammad MA, Cresci GAM. A Designer Synbiotic Attenuates Chronic-Binge Ethanol-Induced Gut-Liver Injury in Mice. *Nutrients*. Jan 5 2019;11(1):97. doi:10.3390/nu11010097

13. Xu S, Zhao M, Wang Q, et al. Effectiveness of Probiotics and Prebiotics Against Acute Liver Injury: A Meta-Analysis. *Front Med (Lausanne)*. 2021;8:739337. doi:10.3389/fmed.2021.739337

14. Lv Z, Guo Y. Metformin and Its Benefits for Various Diseases. *Front Endocrinol (Lausanne)*. 2020;11:191. doi:10.3389/fendo.2020.00191

15. Podhorecka M, Ibanez B, Dmoszynska A. Metformin - its potential anti-cancer and anti-aging effects. *Postepy Hig Med Dosw (Online)*. Mar 2 2017;71(0):170-175. doi:10.5604/01.3001.0010.3801

16. Kang MJ, Moon JW, Lee JO, et al. Metformin induces muscle atrophy by transcriptional regulation of myostatin via HDAC6 and FoxO3a. *J Cachexia Sarcopenia Muscle*. Feb 2022;13(1):605-620. doi:10.1002/jcsm.12833

17. Xiong C, Yin D, Li J, et al. Metformin Reduces Renal Uptake of Radiotracers and Protects Kidneys from Radiation-Induced Damage. *Mol Pharm*. Feb 4 2019;16(2):808-815. doi:10.1021/acs.molpharmaceut.8b01091

18. McCreight LJ, Bailey CJ, Pearson ER. Metformin and the gastrointestinal tract. *Diabetologia*. Mar 2016;59(3):426-35. doi:10.1007/s00125-015-3844-9

19. Sun L, Xie C, Wang G, et al. Gut microbiota and intestinal FXR mediate the clinical benefits of metformin. *Nat Med*. Dec 2018;24(12):1919-1929. doi:10.1038/s41591-018-0222-4

20. Liang H, Song H, Zhang X, et al. Metformin attenuated sepsis-related liver injury by modulating gut microbiota. *Emerg Microbes Infect*. Dec 2022;11(1):815-828. doi:10.1080/22221751.2022.2045876

21. Jiang A, Du P, Liu Y, Pu J, Shi J, Zhang H. Metformin regulates the Th17/Treg balance by glycolysis with TIGAR in hepatic ischemia-reperfusion injury. *J Pharmacol Sci*. May 2021;146(1):40-48. doi:10.1016/j.jphs.2021.01.006

22. Mueller NT, Differding MK, Zhang M, et al. Metformin Affects Gut Microbiome Composition and Function and Circulating Short-Chain Fatty Acids: A Randomized Trial. *Diabetes Care*. Jul 2021;44(7):1462-1471. doi:10.2337/dc20-2257

23. Lee CB, Chae SU, Jo SJ, Jerng UM, Bae SK. The Relationship between the Gut Microbiome and Metformin as a Key for Treating Type 2 Diabetes Mellitus. *Int J Mol Sci*. Mar 30 2021;22(7):3566. doi:10.3390/ijms22073566

24. Liu Z, Liao W, Zhang Z, et al. Metformin Affects Gut Microbiota Composition and Diversity Associated with Amelioration of Dextran Sulfate Sodium-Induced Colitis in Mice. *Front Pharmacol*. 2021;12:640347. doi:10.3389/fphar.2021.640347

25. Milosevic I, Vujovic A, Barac A, et al. Gut-Liver Axis, Gut Microbiota, and Its Modulation in the Management of Liver Diseases: A Review of the Literature. *Int J Mol Sci*. Jan 17 2019;20(2):395. doi:10.3390/ijms20020395

26. Bi J, Zhang J, Ren Y, et al. Irisin alleviates liver ischemia-reperfusion injury by inhibiting excessive mitochondrial fission, promoting mitochondrial biogenesis and decreasing oxidative stress. *Redox Biol*. Jan 2019;20:296-306. doi:10.1016/j.redox.2018.10.019

27. Li X, Wang L, Yang X, Huang C. Metformin Attenuates Ischemia-reperfusion Injury of Fatty Liver in Rats Through Inhibition of the TLR4/NF-kappaB Axis. *Balkan Med J*. Jun 1 2020;37(4):196-202. doi:10.4274/balkanmedj.galenos.2020.2019.9.31

28. Forslund K, Hildebrand F, Nielsen T, et al. Disentangling type 2 diabetes and metformin treatment signatures in the human gut microbiota. *Nature*. Dec 10 2015;528(7581):262-266. doi:10.1038/nature15766

29. Li R, Xie L, Li L, et al. The gut microbial metabolite, 3,4-dihydroxyphenylpropionic acid, alleviates hepatic ischemia/reperfusion injury via mitigation of macrophage pro-inflammatory activity in mice. *Acta Pharm Sin B*. Jan 2022;12(1):182-196. doi:10.1016/j.apsb.2021.05.029

30. Zhang Y, Wu T, Li W, et al. Lactobacillus casei LC89 exerts antidiabetic effects through regulating hepatic glucagon response and gut microbiota in type 2 diabetic mice. *Food Funct*. Sep 20 2021;12(18):8288-8299. doi:10.1039/d1fo00882j

31. Lee H, Lee Y, Kim J, et al. Modulation of the gut microbiota by metformin improves metabolic profiles in aged obese mice. *Gut Microbes*. Mar 4 2018;9(2):155-165. doi:10.1080/19490976.2017.1405209

32. Shi Z, Chen G, Cao Z, et al. Gut Microbiota and Its Metabolite Deoxycholic Acid Contribute to Sucralose Consumption-Induced Nonalcoholic Fatty Liver Disease. *J Agric Food Chem*. Apr 7 2021;69(13):3982-3991. doi:10.1021/acs.jafc.0c07467

33. Liu R, Hong J, Xu X, et al. Gut microbiome and serum metabolome alterations in obesity and after weight-loss intervention. *Nat Med*. Jul 2017;23(7):859-868. doi:10.1038/nm.4358

34. Ikeyama N, Murakami T, Toyoda A, et al. Microbial interaction between the succinate-utilizing bacterium Phascolarctobacterium faecium and the gut commensal Bacteroides thetaiotaomicron. *Microbiologyopen*. Oct 2020;9(10):e1111. doi:10.1002/mbo3.1111

35. Otaru N, Ye K, Mujezinovic D, et al. GABA Production by Human Intestinal Bacteroides spp.: Prevalence, Regulation, and Role in Acid Stress Tolerance. *Front Microbiol*. 2021;12:656895. doi:10.3389/fmicb.2021.656895

36. Schafer DF, Fowler JM, Jones EA. Colonic bacteria: a source of gamma-aminobutyric acid in blood. *Proc Soc Exp Biol Med*. Jul 1981;167(3):301-303. doi:10.3181/00379727-167-41169

37. Wang S, Xiang YY, Zhu J, et al. Protective roles of hepatic GABA signaling in acute liver injury of rats. *Am J Physiol Gastrointest Liver Physiol*. Mar 1 2017;312(3):G208-G218. doi:10.1152/ajpgi.00344.2016

38. Shilpa J, Pretty MA, Anitha M, Paulose CS. Gamma aminobutyric acid B and 5-hydroxy tryptamine 2A receptors functional regulation during enhanced liver cell proliferation by GABA and 5-HT chitosan nanoparticles treatment. *Eur J Pharmacol*. Sep 5 2013;715(1-3):154-163. doi:10.1016/j.ejphar.2013.05.028

39. Clark JW, Daykin H, Metha JA, et al. Manipulation of rapid eye movement sleep via orexin and GABAA receptor modulators differentially affects fear extinction in mice: effect of stable versus disrupted circadian rhythm. *Sleep*. Sep 13 2021;44(9):zsab068. doi:10.1093/sleep/zsab068

40. Zeng K, Xie A, Dong X, et al. GABA-Aalpha5 Might Be Involved in Learning-Memory Dysfunction in the Offsprings of Chronic Ethanol-Treated Rats via GABA-Aalpha5 Histone H3K9 Acetylation. *Front Neurosci*. 2019;13:1076. doi:10.3389/fnins.2019.01076

Figure legends

Figure 1. Metformin significantly mitigates HIRI by reshaping gut microbiota in mice

(a) Survival rate analysis (n = 10-12/group), *Kaplan Meier* was used to analyze statistical differences (Control vs IR, and IR+Met vs IR). (b) Morphological appearance, H&E and PAS staining of liver (n = 3/group). (c) Serum ALT and AST levels. (d) Levels of MDA and GSH in liver tissue. (e) Sobs index, PCoA (n = 4/group). (f) H&E staining of ileum and colon (n = 3/group). (g) Western blot of Occludin in colon (n = 3/group). (h) IFC of ZO-1 and Occludin in colon (n = 3/group). (i) qRT-PCR analysis of *Ocln, Tjp1, Cldn7, F11r* and *Igsf5* in ileum. (j) *Il6, Il1b* and *Il18* in ileum and colon. (n = 3–5/group). (k) FD-4 level in mice serum (n = 3). Data are expressed as mean ± standard deviation. *One-way ANOVA* was used to analyze statistical differences; $*P < 0.05$, $**P < 0.01$ and $***P < 0.001$.

Figure 2. Metformin-reshaped fecal microbiota attenuates HIRI

(a) Survival rate analysis (n = 10-12/group) , *Kaplan Meier* was used to analyze statistical differences. (b) Serum ALT and AST levels. Levels of MDA (c) and GSH (d) in liver tissue. (e) H&E, PAS and DHE staining of liver (n = 3/group). (f) Alpha diversity and PCoA level of mice microbes. (g) H&E staining of ileum and colon and Western blot analysis of Occludin in colon (n = 3/group). (h) IFC of ZO-1 and Occludin in colon (n = 3/group). (i) qRT-PCR analysis of *Ocln, Tjp1, Cldn7, F11r* and *Igsf5* in ileum, and *Il6, Il1b* and *Il18* in ileum and colon. (n = 3–5/group). (j) FD-4 level in mice serum (n = 3). (k) ALT, AST and MDA detection between Control and Control + Abx group; survival rate of IR + Met + Abx group (n = 10) , *Kaplan Meier* was used to analyze statistical differences ; and the levels of serum ALT, AST, liver MDA, Fe, and GSH in IR + Met + Abx group. Data are expressed as mean ± standard deviation. *One-way ANOVA* was used to analyze statistical differences; $*P < 0.05$, $**P < 0.01$ and $***P < 0.001$.

Figure 3. Metformin alleviates HIRI through inhibiting ferroptosis

(a) Levels of Fe in liver tissue (n=6). qRT-PCR analysis of *Acsl4* (b) *Slc7a11* (c), *Slc39a14* (d) and *Ptgs2* (e) (n = 5-8/group). (f) Western blot analysis of ACSL4, FTH1, VDAC1, VDAC2, VDAC3, TFR1 and Xct in liver tissue (n = 3/group). (g) Lipid ROS staining and TEM analysis of liver tissues (n = 3/group). (h) Ferroptosis-related transcriptome cluster diagram heatmap. Data are expressed as mean ± standard deviation. *One-way ANOVA* was used to analyze statistical differences; $*P < 0.05$, $**P < 0.01$ and $***P < 0.001$.

Figure 4. Metformin induces GABA-producing gut microbiota.

(a) KEGG analysis of transcriptome. (b). HPLC-MS/MS of GABA content in liver, ELISA of GABA in liver (n = 6–9/group). (c) Community heatmap analysis on genus level. (d) qRT-PCR analysis of key metabolite enzyme glutamate decarboxylase 1 (*Gad1*), glutamic acid decarboxylase 2 (*Gad2*), 4-aminobutyrate aminotransferase (*Abat*), aldhehyde dehydrogenase family 5 *(Aldh5a1*) in liver (n = 5-8/group). (e) ELISA of GABA in feces (n = 7–10/group) (f) Western-blot analysis of GAD1 and GAD2 in liver. (g-h) qRT-PCR analysis of GAD and PAT in mice feces (n= 3-5/group). (i) Metagenomic sequencing analysis of human feces. (j-k) The level of GAD, PAT, GABA and Glu in human feces (n= 5-6/group) l) The level of GABA, Glu and putrescine in human feces vitro culture (n= 3/group). Data are expressed as mean ± standard deviation. *One-way ANOVA* was used to analyze statistical differences; $*P < 0.05$, $**P < 0.01$ and $***P < 0.001$.

Figure 5. GABA is the critical metabolite of metformin-reshaped gut microbiota against HIRI-induced ferroptosis.

(a) Diagram of GABA treatment experiment on mice model. (b) H&E and PAS staining of liver (n = 3/group). (c) Serum ALT and AST levels (n =6/group). Levels of MDA, GSH and Fe in liver tissues (d) (n =4/group). (e) Western blot analysis of ASCL4, FTH1, TFR1 and VADC1,2,3 in liver (n = 4/group). (f) Ferroptosis-related transcriptome cluster diagram

heatmap (n = 3-5/group). Data are expressed as mean ± standard deviation. *One-way ANOVA* was used to analyze statistical differences; *$P < 0.05$, **$P < 0.01$ and ***$P < 0.001$.

Supplementary files figure legends

Figure 1- source data 1: Original file for the Western blot analysis in Figure 1g.

Figure 1- source data 2: PDF containing Figure 1g and original scans of the relevant Western blot analysis with highlighted bands and sample labels.

Figure 2- source data 1: Original file for the Western blot analysis in Figure 2g.

Figure 2- source data 2: PDF containing Figure 2g and original scans of the relevant Western blot analysis with highlighted bands and sample labels.

Figure 3- source data 1: Original file for the Western blot analysis in Figure 3f.

Figure 3- source data 2: PDF containing Figure 3f and original scans of the relevant Western blot analysis with highlighted bands and sample labels.

Figure 4- source data 1: Original file for the Western blot analysis in Figure 4f.

Figure 4- source data 2: PDF containing Figure 4f and original scans of the relevant Western blot analysis with highlighted bands and sample labels.

Figure 5- source data 1: Original file for the Western blot analysis in Figure 5e.

Figure 5- source data 2: PDF containing Figure 5e and original scans of the relevant Western blot analysis with highlighted bands and sample labels.

Supplementary file 1: Excel file containing the sequence list of relevant mouse genes.

Supplementary file 2: Excel file containing the source list of antibiotics used in the article.

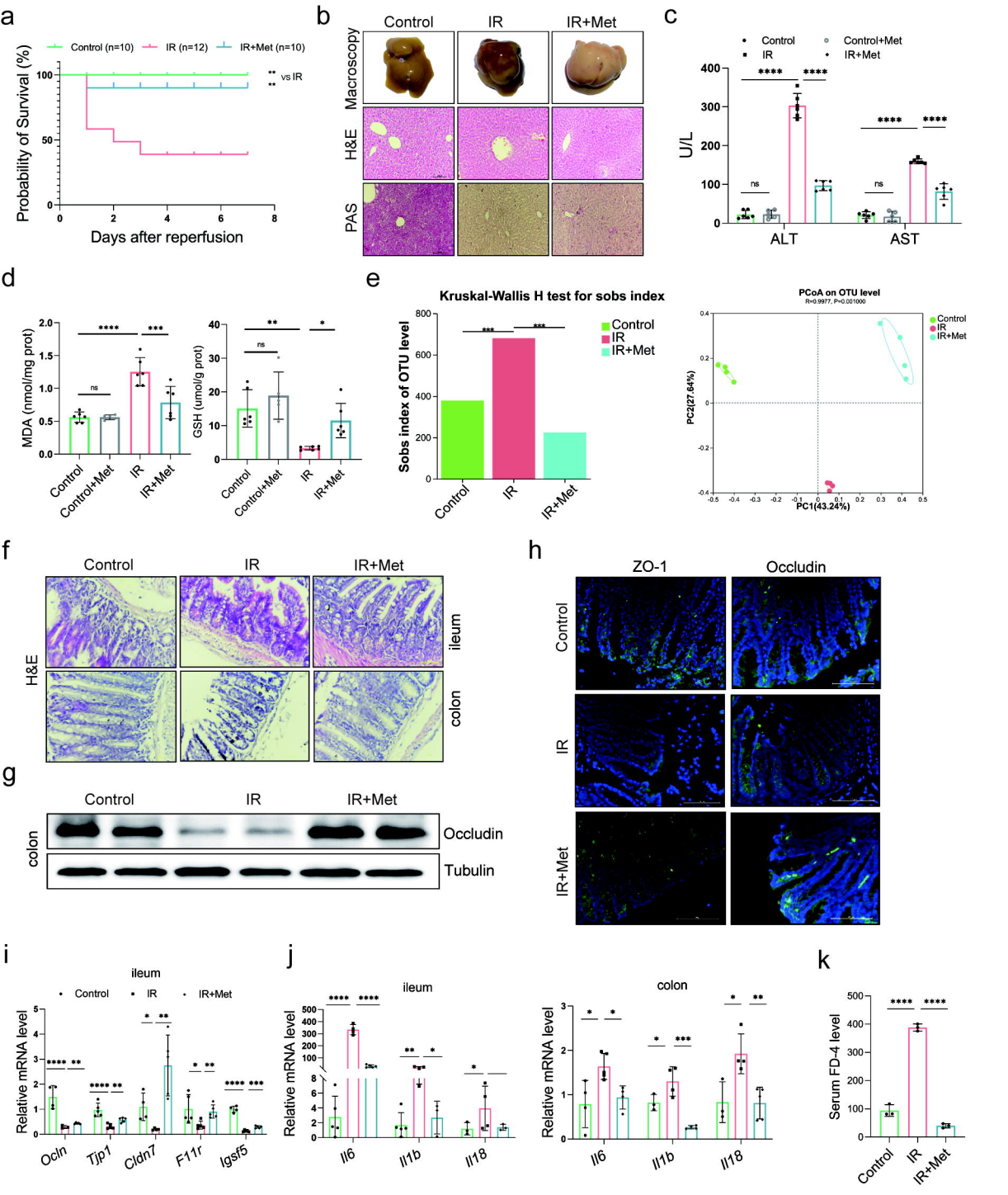
a
Control (n=10)
IR (n=12)
IR+Met (n=10)
** vs IR
**
Probability of Survival (%)
Days after reperfusion
b
Control
IR
IR+Met
Macroscopy
H&E
PAS
c
Control
IR
Control+Met
IR+Met
U/L
ALT
AST
ns
d
MDA (nmol/mg prot)
GSH (umol/g prot)
Control
Control+Met
IR
IR+Met
e
Kruskal-Wallis H test for sobs index
Sobs index of OTU level
PCoA on OTU level
R=0.9977, P=0.001000
PC1(43.24%)
PC2(27.64%)
f
Control
IR
IR+Met
H&E
ileum
colon
g
Control
IR
IR+Met
colon
Occludin
Tubulin
h
ZO-1
Occludin
Control
IR
IR+Met
i
ileum
Control
IR
IR+Met
Relative mRNA level
Ocln
Tjp1
Cldn7
F11r
Igsf5
j
ileum
colon
Relative mRNA level
Il6
Il1b
Il18
k
Serum FD-4 level
Control
IR
IR+Met

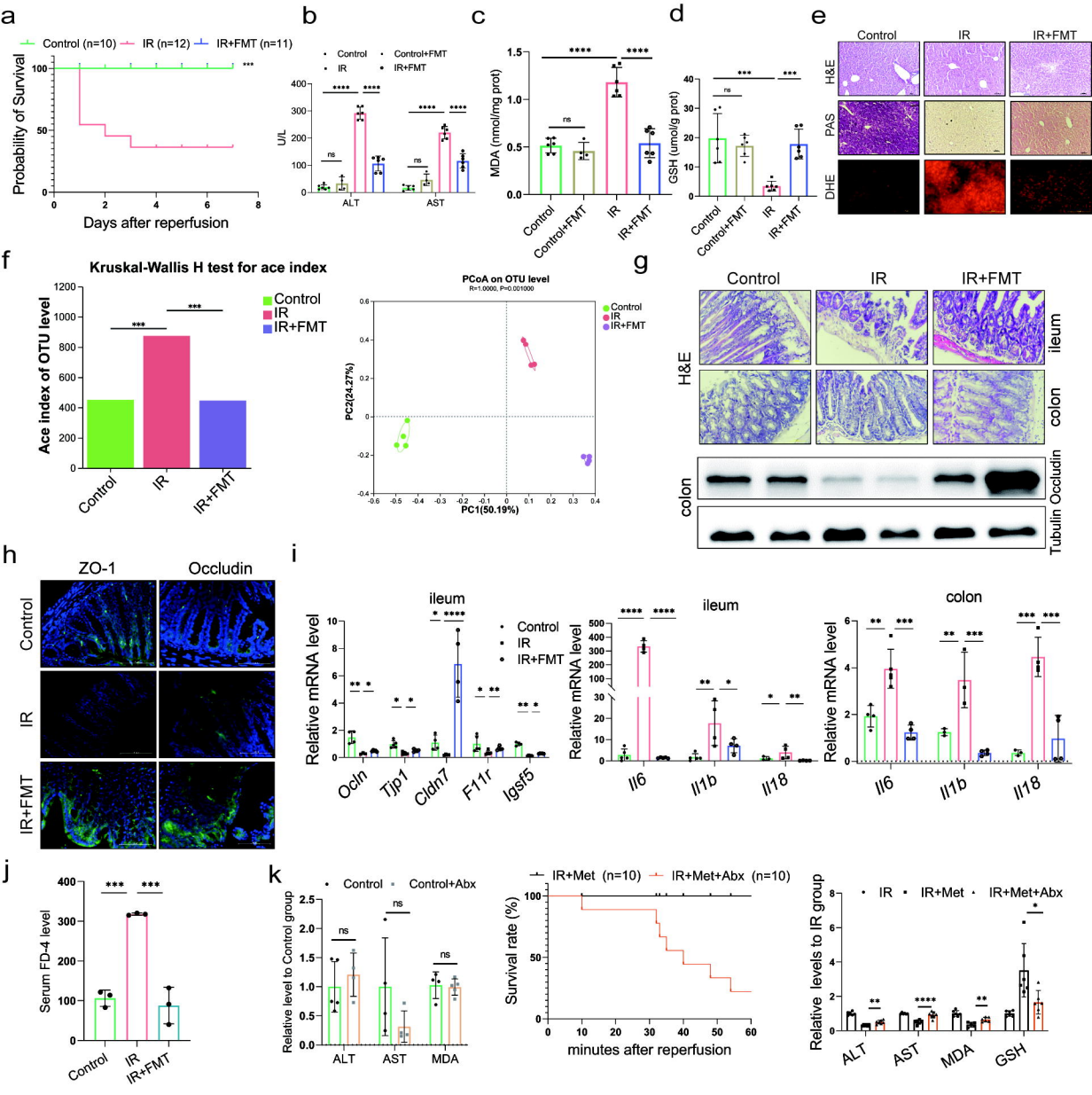
a
Control (n=10)
IR (n=12)
IR+FMT (n=11)
Probability of Survival
Days after reperfusion
b
Control
Control+FMT
IR
IR+FMT
U/L
ALT
AST
c
MDA (nmol/mg prot)
Control
Control+FMT
IR
IR+FMT
d
GSH (umol/g prot)
e
Control
IR
IR+FMT
H&E
PAS
DHE
f
Kruskal-Wallis H test for ace index
Ace index of OTU level
PCoA on OTU level
R=1.0000, P=0.001000
PC2(24.27%)
PC1(50.19%)
g
ileum
colon
Occludin
Tubulin
h
ZO-1
Occludin
i
Relative mRNA level
Ocln
Tjp1
Cldn7
F11r
Igsf5
Il6
Il1b
Il18
j
Serum FD-4 level
k
Control+Abx
Relative level to Control group
IR+Met (n=10)
IR+Met+Abx (n=10)
Survival rate (%)
minutes after reperfusion
IR+Met
IR+Met+Abx
Relative levels to IR group
GSH

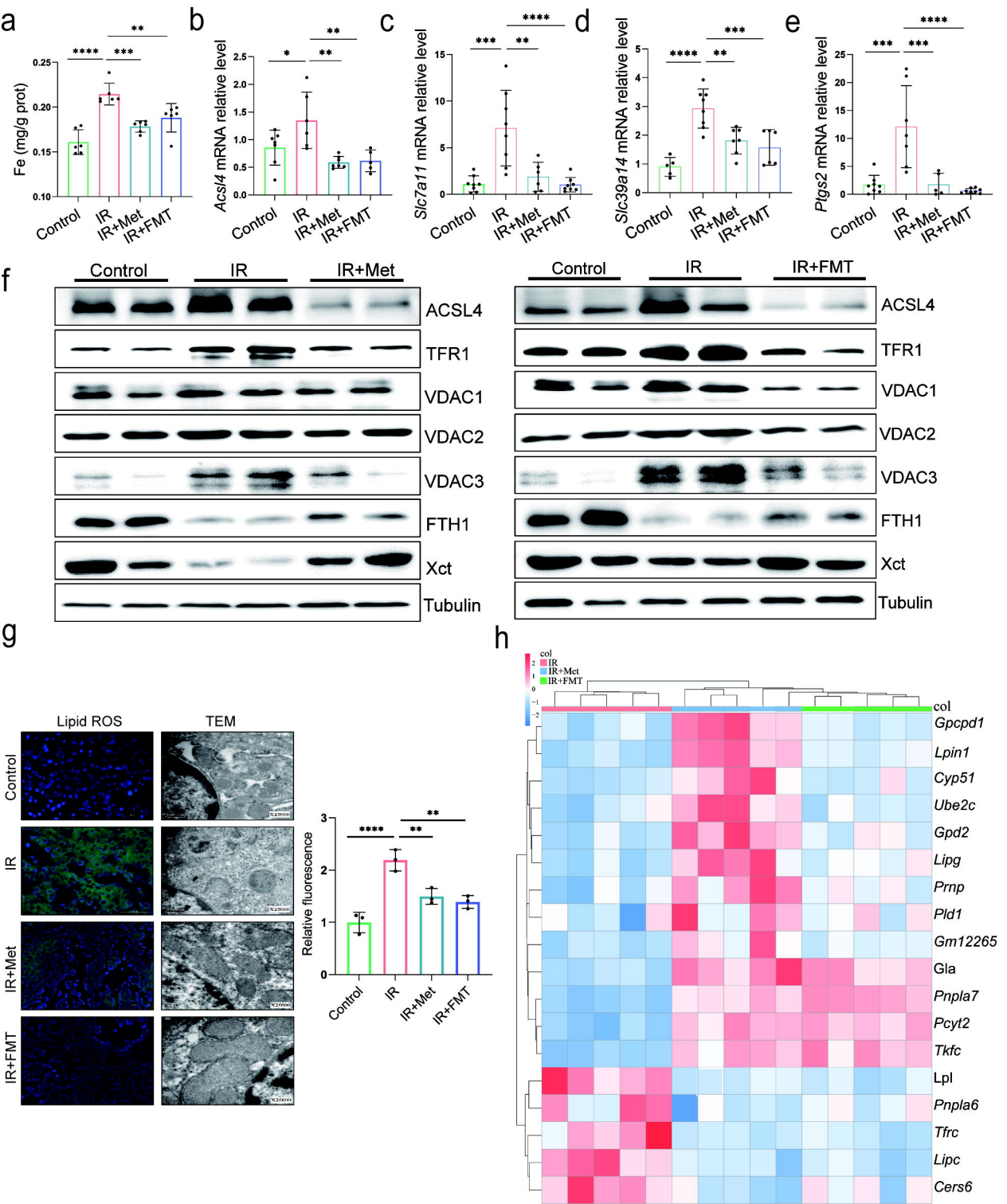
a
Fe (mg/g prot)
Control
IR
IR+Met
IR+FMT
b
Acsl4 mRNA relative level
c
Slc7a11 mRNA relative level
d
Slc39a14 mRNA relative level
e
Ptgs2 mRNA relative level
f
ACSL4
TFR1
VDAC1
VDAC2
VDAC3
FTH1
Xct
Tubulin
g
Lipid ROS
TEM
Relative fluorescence
h
col
Gpcpd1
Lpin1
Cyp51
Ube2c
Gpd2
Lipg
Prnp
Pld1
Gm12265
Gla
Pnpla7
Pcyt2
Tkfc
Lpl
Pnpla6
Tfrc
Lipc
Cers6

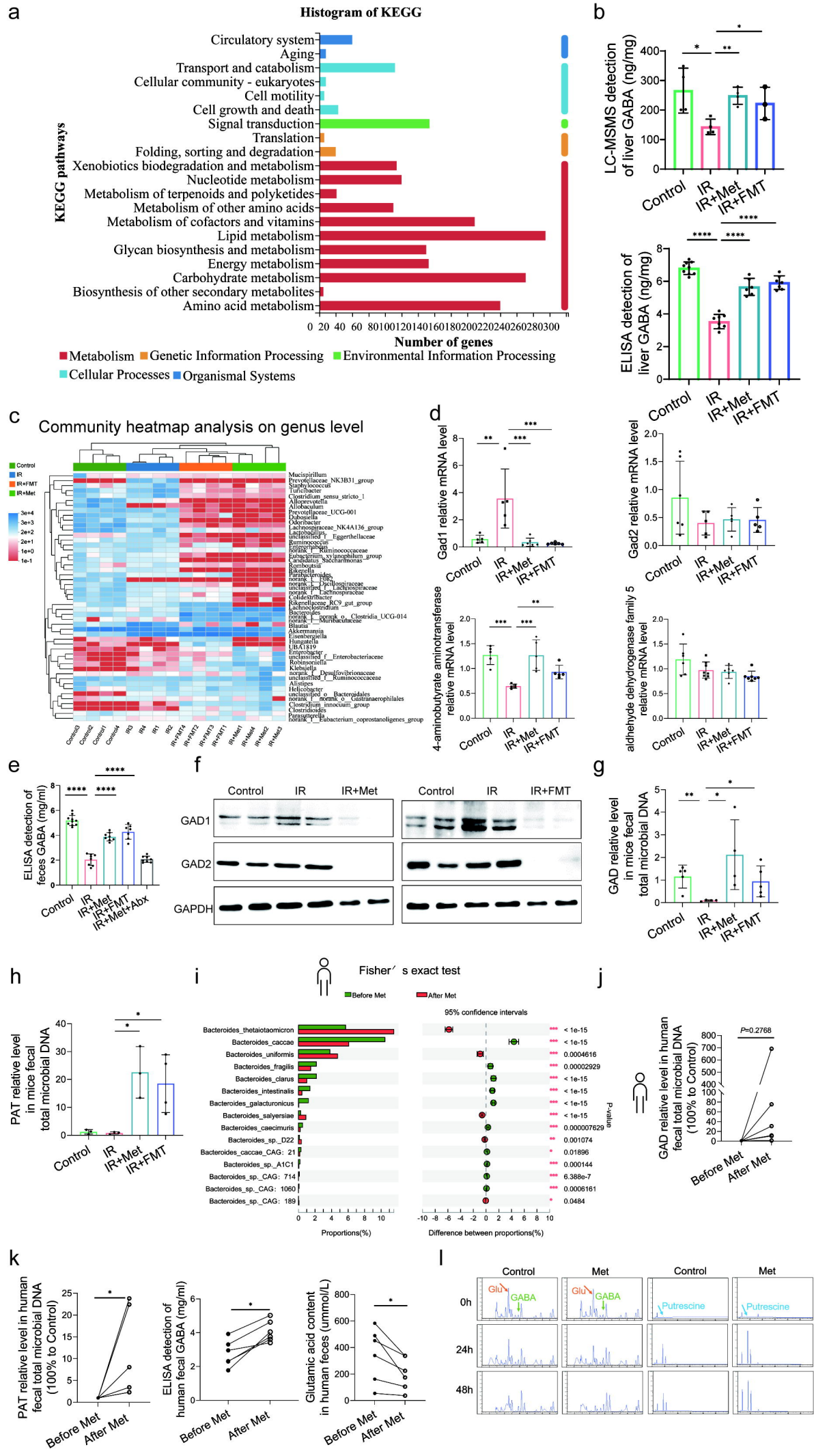
a
Histogram of KEGG
KEGG pathways
Circulatory system
Aging
Transport and catabolism
Cellular community - eukaryotes
Cell motility
Cell growth and death
Signal transduction
Translation
Folding, sorting and degradation
Xenobiotics biodegradation and metabolism
Nucleotide metabolism
Metabolism of terpenoids and polyketides
Metabolism of other amino acids
Metabolism of cofactors and vitamins
Lipid metabolism
Glycan biosynthesis and metabolism
Energy metabolism
Carbohydrate metabolism
Biosynthesis of other secondary metabolites
Amino acid metabolism
0 20 40 60 80 100 120 140 160 180 200 220 240 260 280 300
Number of genes
Metabolism
Genetic Information Processing
Environmental Information Processing
Cellular Processes
Organismal Systems
b
LC-MSMS detection of liver GABA (ng/mg)
Control
IR
IR+Met
IR+FMT
ELISA detection of liver GABA (ng/mg)
c
Community heatmap analysis on genus level
Control
IR
IR+FMT
IR+Met
d
Gad1 relative mRNA level
Gad2 relative mRNA level
4-aminobutyrate aminotransferase relative mRNA level
aldehyde dehydrogenase family 5 relative mRNA level
e
ELISA detection of feces GABA (mg/ml)
IR+Met+Abx
f
Control
IR
IR+Met
IR+FMT
GAD1
GAD2
GAPDH
g
GAD relative level in mice fecal total microbial DNA
h
PAT relative level in mice fecal total microbial DNA
i
Fisher´s exact test
Before Met
After Met
95% confidence intervals
Bacteroides_thetaiotaomicron
Bacteroides_caccae
Bacteroides_uniformis
Bacteroides_fragilis
Bacteroides_clarus
Bacteroides_intestinalis
Bacteroides_galacturonicus
Bacteroides_salyersiae
Bacteroides_caecimuris
Bacteroides_sp._D22
Bacteroides_caccae_CAG: 21
Bacteroides_sp._A1C1
Bacteroides_sp._CAG: 714
Bacteroides_sp._CAG: 1060
Bacteroides_sp._CAG: 189
P-value
Proportions(%)
Difference between proportions(%)
j
GAD relative level in human fecal total microbial DNA (100% to Control)
P=0.2768
k
PAT relative level in human fecal total microbial DNA (100% to Control)
ELISA detection of human fecal GABA (mg/ml)
Glutamic acid content in human feces (ummol/L)
Before Met
After Met
l
Control
Met
0h
24h
48h
Glu
GABA
Putrescine

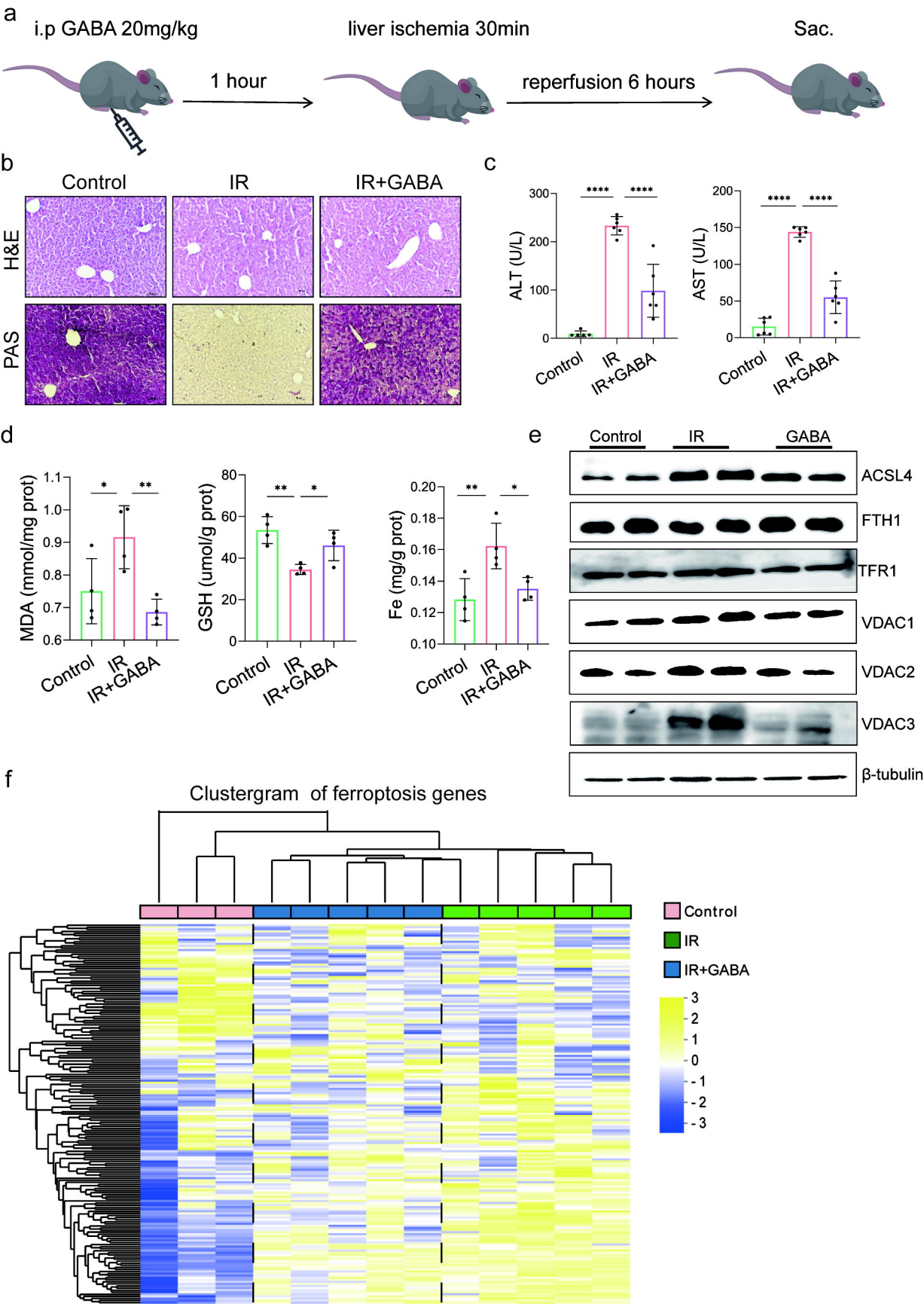
a
i.p GABA 20mg/kg
1 hour
liver ischemia 30min
reperfusion 6 hours
Sac.
b
Control
IR
IR+GABA
H&E
PAS
c
ALT (U/L)
AST (U/L)
****
Control
IR
IR+GABA
d
MDA (mmol/mg prot)
GSH (umol/g prot)
Fe (mg/g prot)
*
**
e
Control
IR
GABA
ACSL4
FTH1
TFR1
VDAC1
VDAC2
VDAC3
β-tubulin
f
Clustergram of ferroptosis genes
Control
IR
IR+GABA